ISSN 1063-7788, Physics of Atomic Nuclei, 2021, Vol. 84, No. 6, pp. 826–836. © Pleiades Publishing, Ltd., 2021.

NUCLEI
Theory

Cubic Interaction and Triaxiality in $^{236-246}$Pu Nuclei

Ashwaq F. Jaafer[1)] and Falih H. Al-Khudair[1)*]

Received April 14, 2021; revised May 25, 2021; accepted May 27, 2021

Abstract—In the present study, we investigate even–even $^{236-246}$Pu isotopes with triaxial interacting boson model. Calculations for the energy levels and $E2$ transition probability were performed using the cubic terms. The study of the influence of cubic $[d \times d \times d]$ and quadrupole $[Q \times Q \times Q]$ interactions on the structure of these nuclei is undertaken. The potential energy surfaces as functions of the deformation parameters were calculated. It has been demonstrated how the cubic term $L = 3$ gives rise to a number of the observed properties of the Pu-nuclei. The comparison between the model results and available experimental data have shown that the structure of these nuclei can be investigated by an $SU(3)$ Hamiltonian.

DOI: 10.1134/S1063778821130123

1. INTRODUCTION

The nuclei with the mass number $A > 200$ have been the subject of various theoretical and experimental studies due to their unique structure and properties. This was a decisive factor in a revival of interest in it so may provide rich references of data for researchers. We cite several experimental [1–13]. Theoretically, there has been wide investigation in an attempt to study their structures, stability, and other properties [14–18]. In the earlier version of Interacting Boson Model IBM-1, the collective states can be reduced to a system of N_B identical bosons. These bosons are the s-boson, with angular momentum $L = 0$, and the d-boson with angular-momentum $L = 2$ state [19–22]. The study by Wilets and Jean [23] confirmed that the degrees of freedom of the deformation parameter play an important role in determining the geometric shape of nuclei in which quadrupole deformities occur. To give the geometric image of the nucleus in its excited collective states, Bohr and Mottelson explained through their geometric model that the shape of the nucleus deviates from the axial symmetry [24].

The Interaction Boson Model (IBM) Hamiltonian has been solved in the Hartree–Fock approximation and that can be seen as a link between the IBM and the geometric model [25–28]. In terms of the quadrupole shape variable, a pictorial representation of the IBM Hamiltonian can be produced through the energy surface derived by taking the expectation value of the IBM Hamiltonian in the intrinsic state. This can give us an idea of the equilibrium and stability of the nucleus [29]. Anther investigation about so-called classical limit by Isacker and Chen [30] including derived a Hamiltonian for each $U5$, $SU(3)$, and $O(6)$ dynamic symmetry. The issue of high-order interaction of d-boson state then has been considered. As well as proved that the stable shapes are shown by the classical limit of IBM Hamiltonian not to be stable triaxial shapes. Heyde et al. [31] show that by incorporating cubic terms in the Hamiltonian of the IBM, one may obtain a stable triaxially shaped nucleus and study the influence of such terms on the energy spectrum in each of the three dynamic symmetries. These analyses were completely restricted to the IBM-1. In contrast Dieperink and Bijker [28, 32] confirmed that triaxiality also occurs in particular dynamic symmetries of the IBM-2 that does distinguish between protons and neutrons.

A three-body interaction between the d-bosons has been included to the Hamiltonian of several nuclei, heavy $_{76}$Os and $_{78}$Pt isotopes were studied. The signature splitting of the γ-vibration band and $B(E2)$ transition were analyzed. It was shown that in none of the nuclei evidence for a stable, triaxial ground-state shape is found [33]. The interacting boson model of Arima and Iachello has been foundational to the description of rotational band in two ^{156}Gd and ^{234}U isotopes. Moreover, the Hamiltonian for 2 and 4-body interaction had been discussed [34].

In the present work of $^{236-246}$Pu investigating, the structure of band levels, electric quadrupole transition rates $B(E2)$, and Potential Energy Surfaces (PES) are purposed. However, the main goal is to determine the effect of three-body boson interactions. Furthermore, we also calculate the PES and the role of three-body interaction in existing of stable triaxial shape within the specified quadrupole deformation

[1)]Department of Physics, College of Education for Pure Sciences, University of Basrah, Basrah, Iraq.
[*]E-mail: falih9@gmail.com

parameters. We will show the behavior of the PES as a function of the deformation angle γ concerning a χ degree of freedom.

2. INTERACTING BOSON MODEL

The contributions of the interacting boson model are very important in describing the heavy and superdeformed structure nuclei [35–37]. Here, we provide some detailed analysis of interactions between bosons. In the first version of Arima and Iachello IBM [19–21], two types of bosons are considered: the s-boson, with angular momentum $L = 0$, and the d-boson with angular-momentum $L = 2$ state. In a given nucleus a total number of bosons is conserved, i.e., the number of creation and annihilation boson operators are equal. The ability to describe the nuclear structure by connection with the group $U(6)$ of unitary transformation in six dimensions is one of the major advantages of the model. However, the nuclei which exhibit collective properties have already been classified by geometric model [38] into vibrational and rotational properties. The interacting boson model can be described analytically by producing a Hamiltonian within the second quantized formula for a system of creation and annihilation boson operators. Because the total number of bosons are conserved by IBM-1 Hamiltonian, this leads to being written in terms of 36 operators [39]:

$$G_k^{(k)}(l,l)' = [b_l^\dagger \times \tilde{b}_{l'}]_k^{(k)} \quad (1)$$
$$= \sum_{\mu_1\mu_2} \langle l\mu_1 l'\mu_2' | Kk\rangle b_{l\mu_1}^\dagger (-1)^{\mu_2'} \tilde{b}_{l',-\mu_2'},$$

where $\tilde{b}_{l'}(b_l^\dagger)$ represents the annihilation (creation) operators of s- and d-boson with $(l, l') = 0$ and 2 angular momenta respectively. We will obviate the delve into the $U(6)$ algebra and its subalgebra but suffice it to say that IBM has three dynamic symmetries contained in the group $U(6)$, the vibrational symmetry $U(5)$ describes spherical nuclei, rotational symmetry $SU(3)$ describes axially deformed nuclei and transitional symmetry describes γ-unstable nuclei [39, 40]. The general form of the Hamiltonian operator of bosons' interactions:

$$\hat{H} = H^{(1)} + H^{(2)} + H^{(3)}, \quad (2)$$

where $H^{(1)}$ includes only one-body terms is given by:

$$H^{(1)} = \epsilon_s [s^\dagger \times s]^{(0)} + \epsilon_d \sqrt{5} [d^\dagger \times \tilde{d}]^{(0)}, \quad (3)$$

the superscription on the rhs refers to the bosons which coupling in zero angular momentum. The first and second terms in Eq. (2) can be written as [29]:

$$\hat{H}_{sd} = \varepsilon_s s^\dagger \cdot s + \varepsilon_d \sum_\mu d_\mu^\dagger \cdot \tilde{d}_\mu + \frac{1}{2} u_0 [(s^\dagger \times s^\dagger)^0 \quad (4)$$
$$\times (s \times s)^0]^{(0)} + u_2 [(d^\dagger \times s^\dagger)^2 \times (\tilde{d} \times s)^2]^{(0)}$$
$$+ \frac{1}{\sqrt{2}} \tilde{\nu}_0 [(d^\dagger \times d^\dagger)^0 \times (s \times s)^0 + (s^\dagger \times s^\dagger)^0$$
$$\times (\tilde{d} \times \tilde{d})^0]^{(0)} + \tilde{\nu}_2 [(d^\dagger \times d^\dagger)^2 \times (\tilde{d} \times s)^2$$
$$+ (d^\dagger \times s^\dagger)^2 \times (\tilde{d} \times \tilde{d})^2]^{(0)} + \sum_{L=0,2,4} \frac{1}{2} (2L+1)^{1/2}$$
$$\times C_L [(d^\dagger \times d^\dagger)^{(L)} \times (\tilde{d} \times \tilde{d})^{(L)}]^{(0)}.$$

To specify the two-body interaction parameters for the Hamiltonian, it is possible to use the "multipole expansion" of the Hamiltonian [41]:

$$H_{sd} = \epsilon_d \hat{n}_d + a_0 \hat{P}\hat{P} + a_1 \hat{L}\hat{L} \quad (5)$$
$$+ a_2 \hat{Q}\hat{Q} + a_3 \hat{T}_3 \hat{T}_3 + a_4 \hat{T}_4 \hat{T}_4,$$

where ϵ_d represents the d-boson energy, $\hat{n}_d$ is the d-boson number operator and $\hat{L} = \sqrt{10}[d^\dagger \times \tilde{d}]^{(1)}$ is the angular momentum operator. The $\hat{P}$ and $\hat{Q}$ represent the paring and quadrupole operators, where:

$$\hat{P} = \frac{1}{2}[(\tilde{d} \cdot \tilde{d}) - (s \cdot s)], \quad (6)$$

$$\hat{Q} = [d^\dagger \times s + s^\dagger \times \tilde{d}]^{(2)} - \chi d^\dagger \times \tilde{d}]^{(2)}. \quad (7)$$

The χ is a shape parameter. The last two terms $\hat{T}_r = [d^\dagger \times \tilde{d}]^{(r)} (r = 3 \text{ and } 4)$ are the octopole and hexadropole operators, respectively. For triaxiality, there is a long history in the theoretical description of the nuclear structure which helps to think about the influence of the cubic term on the energy spectra and consequently the shape of nuclei [26, 29, 30]. By incorporating the three-body terms in the Hamiltonian of the IBM-1, we can understand a triaxial behavior in nuclei that exhibit a triaxial minimum in the potential energy surfaces at the nuclei equilibrium shape. The third term $H^{(3)}$ in Eq. (2) represents three-body interaction [33]:

$$H^{(3)} = \sum_L \tilde{v}^L_{l_1 l_2 l_3 l_1' l_2' l_3'} [[d^\dagger \times d^\dagger]^{(\lambda)} \times d^\dagger]^{(L)} \quad (8)$$
$$\times [[\tilde{d} \times \tilde{d}]^{(\lambda)'} \times \tilde{d}]^{(L)}.$$

There are 17 linear independent combinations. So, we can find five linear combinations of the type $(d^\dagger d^\dagger d^\dagger)^{(L)} \cdot (\tilde{d}\tilde{d}\tilde{d})^{(L)}$, where $(L = 0, 2, 3, 4, 6)$ and $(\lambda = 0, 2, 4)$ (for more details see [33, 42]).

The triaxial effects will appear explicitly if we modify Hamiltonian in Eq. (4) this can be described through an equation such as the following:

$$\hat{H} = H_{sd} + \sum_L \theta_L [d^\dagger d^\dagger d^\dagger]^{(L)} \cdot (\tilde{d}\tilde{d}\tilde{d})^{(L)}, \quad (9)$$

Table 1. Hamiltonians' parameter values (in MeV unit) used for the description energy scheme of the Plutonium isotopes chain, $\theta_3 = -0.004$ MeV, and $q_3 = 0.0001$ MeV and $\chi = -1.3227$ for all isotopes

Isotopes	^{236}Pu	^{238}Pu	^{240}Pu	^{242}Pu	^{244}Pu	^{246}Pu
N_B	14	15	16	17	18	19
a_1	0.0018	0.0020	0.003	0.0036	0.0042	0.0050
a_2	−0.0130	−0.0110	−0.0080	−0.0066	−0.0060	−0.0060

Table 2. The parameters' value of electric transition operator in (eb) unit

Isotopes	^{236}Pu	^{238}Pu	^{240}Pu	^{242}Pu	^{244}Pu	^{246}Pu
α_2	0.159	0.151	0.143	0.139	0.133	0.127
β_2	−0.240	−0.230	−0.220	−0.210	−0.200	−0.190

where θ_L ($L = 0, 2, 3, 4, 6$) represent the interaction parameters most often used to describe the triaxiality. The presence of the cubic term $L = 3$ is so necessary to achieve stable triaxial shapes in the potential energy surfaces [31].

With $(\hat{Q} \times \hat{Q} \times \hat{Q})^{(0)}$ term based on the third-order moments of quadrupole operator in the ground state within ($L = 0$) degree of triaxiality [43–47], the total Hamiltonian can be written as:

$$\hat{H} = a_1(\hat{L} \cdot \hat{L}) + a_2(\hat{Q} \cdot \hat{Q}) \qquad (10)$$
$$+ \sum_{\lambda L} \theta_L[(d^\dagger \times d^\dagger)^{(\lambda)} \times d^\dagger]^{(L)} \cdot [(\tilde{d} \times \tilde{d})^{(\lambda)} \times \tilde{d}]^{(L)}$$
$$- q_3[\hat{Q} \times \hat{Q} \times \hat{Q}]^{(0)}.$$

3. RESULTS AND DISCUSSION

3.1. Energy Levels

Firstly, we would like to ensure before going into highlight and comment on a nuclear structure of Plutonium isotopes, whether it has an exact $SU(3)$ limit referred by the typical energy ratio $E_{4_1^+}/E_{2_1^+} = 3.333$ and bands position [20]. Secondly, $^{236-246}$Pu isotopes have neutron number $N = 142–152$. To produce a deformed structure of Pu isotopes, it is of course necessary to determine the a_1 and a_2 parameters. The energy values of the ground band are close to those of the $J(J+1)$ rotor spectra. The variety of system parameters and $E2$ transition parameters have been listed in Tables 1 and 2. These values served as a powerful tool to reproduce more close results to those of available experimental [48]. Within Eq. (10) we have implicitly three Hamiltonians taken into account. The $H_{\rm IBM}$, is a standard $SU(3)$ Hamiltonian which includes only the angular momentum and quadrupole interaction terms (a_1 and a_2) [5, 49]. The $H_{\rm IBMC}$ represents the calculation with a_1, a_2 and θ_3. While $H_{\rm IBMCQ}$ represents the calculations with a_1, a_2, θ_3 and q_3. The eigenvalue problem of the Hamiltonian can be solved by numerical diagonalization utilizing the IBM code [51]. The results of the IBM, IBMC, IBMCQ for the ground state, and other excited states energy for the nuclei being examined were calculated. Here we have six energy level schemes, and the rich experimental data ^{240}Pu scheme has been plotted in Fig. 1.

A good agreement between the IBM and EXP results is observed in g.s-band levels. Overall as seen in Fig. 1, the energy value of β-band levels ($K = 0$) are affected hardly by adding the cubic term. In contrast, the levels of γ-band ($K = 2$) had risen as a result of adding $L = 3$ term. Turning now to the specific action of adding cubic quadrupole term to Hamiltonian Eq. (9) with the a_1, a_2, θ_3, and q_3 parameters would produce a significant risen in energies' level of γ-band moreover the β and g.s.-band. For $N = 142–152$ the difference in energy between IBM and IBMC results for γ-band particularly at high angular momentum $I^\pi = 24^+$ is 0.15, 0.17, 0.20, 0.23, 0.26, and 0.29 MeV. For $J^\pi = 25^+$ is 0.22, 0.24, 0.26, 0.28, 0.31, and 0.34 MeV, respectively.

Towards middshell ($N = 152$), the difference in energy was found at angular momentum $J^\pi = 29^+$ and 30^+ equal to 0.37 and 0.28 MeV, respectively. For γ-band levels, it should be noted that at high odd-J they are more affected by the cubic term and the operator of the cubic quadrupole than at even-J. Therefore, we will collect a clustering pattern which leads to a slightly odd-even staggering observed at $J^\pi \geqslant 15^+$ from IBMC furthermore IBMCQ calculation. For example, the γ-band energy levels cluster as $(15_\gamma^+, 16_\gamma^+)$, $(17_\gamma^+, 18_\gamma^+)$, and so on [52]. Also, the

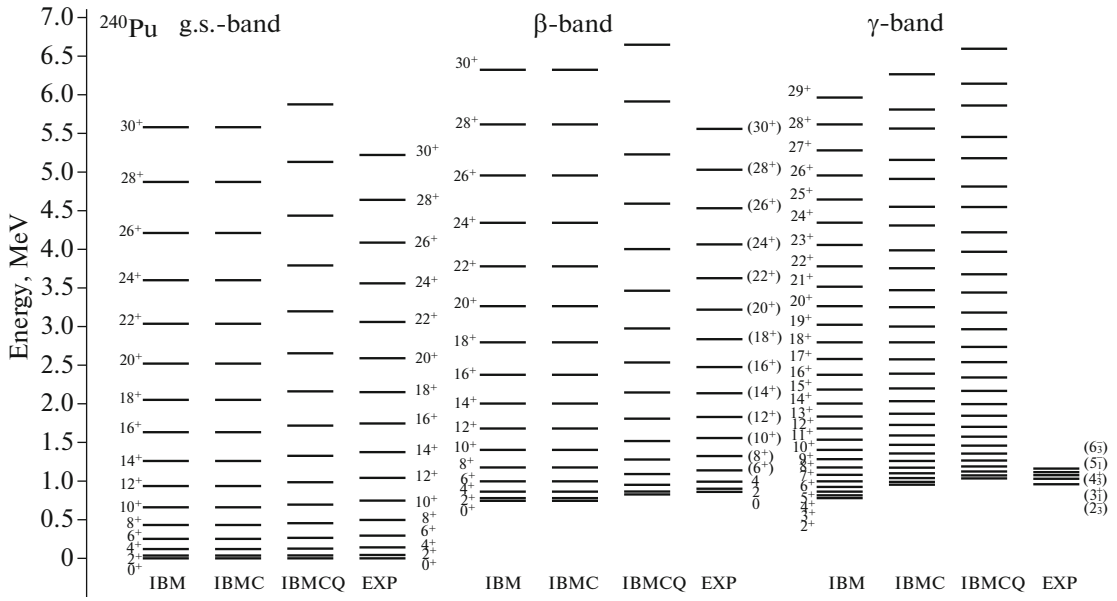

Fig. 1. Comparison of calculated energy levels of ^{240}Pu isotope with available experimental data [48].

energy spacing between each pair of these levels is almost equal. We have observed in ^{240}Pu calculations, that the theoretical results for this isotope seem to be consistent with available experimental data of γ- and β-band levels. Clearly for the low-lying β-band, the IBMCQ results in good agreement with experimental ones. On the other hand, the IBMC results are consistent with available experimental data.

3.2. Electric Quadrupole Transition Probability

The IBM electric quadrupole transition can be written as [22, 53–55]:

$$T(E2) = \alpha_2[d^\dagger \times s + s^\dagger \times \tilde{d}]^{(2)} + \beta_2[d^\dagger \times \tilde{d}]^{(2)}, \quad (11)$$

the matrix elements in Eq. (11) are calculated using the wave functions of the states generated by the energy level calculation. Knowing the reduced matrix element ($\langle J_f||T(E2)||J_i\rangle$), one can directly determine the electric transition probability $B(E2)$:

$$B(E2; J_i \to J_f) = \frac{(\langle J_f||T(E2)||J_i\rangle)^2}{2J_i + 1}. \quad (12)$$

The value of α_2 parameter is estimated to reproduce the experimental value $B(E2; 2_1^+ \to 0_1^+)$, the β_2 is taken negative to achieve the selection rules for intraband and interband transitions [56]. The $B(E2)$ values for $^{236-246}$Pu isotopes have been listed in Tables 3 and 4. From these tables, it can be seen that the $B(E2; 2_1^+ \to 0_1^+)$ values increase with the number of bosons. The theoretical values are in good agreement with available experimental data [48]. From the $B(E2)$ values, one can see that $B(E2; (8_1^+ \to 6_1^+))$ value is stronger as compared to other $g \to g$ transition, furthermore $\beta \to \beta$ and $\gamma \to \gamma$ transition. For high spin states, the transitions decreased progressively, possibly due to the occurrence of backbending in yrast spectra [57].

However, we note the currently available $\beta \to g$ and $\gamma \to g$ transitions have vanished [22] in both IBM, IBMC, and IBMCQ calculations. Closer inspection of the IBM, IBMC results in Tables 1, 2 shows very weak transitions. Moreover, in IBM calculation there is a clear trend of increasing the $\gamma_{\text{even}} \to \gamma_{\text{even}}$ transitions but faling in value when $L = 3$ is included. As Fig. 2 clarifies, the $B(E2)$ values are larger in ^{236}Pu and ^{244}Pu than in other isotopes, since in $SU(3)$ symmetry they increase as N^2.

The results obtained from the IBM and IBMC calculations for the ratio $B_\beta = \dfrac{B(E2; 4_2^+ \to 4_1^+)}{B(E2; 4_2^+ \to 2_2^+)}$ are shown in Fig. 3*a*, with the cubic term, it has values flowing from $(7.29 \text{ to } 6) \times 10^{-5}$ at $N = 142$, 152 respectively. Without this term, the ratio B_β has a maximum value at $N = 146$. In Fig. 3*b*, there is a clear trend of increase in $B_\gamma = \dfrac{B(E2; 3_1^+ \to 4_1^+)}{B(E2; 3_1^+ \to 2_2^+)}$ according to IBMC calculation and it stoops at $N = 146$ with value $B_\gamma = 4.5 \times 10^{-2}$, beyond this point, it decreases slowly with increasing neutron number. In IBM, the behavior is like in IBMC, but the increasing breaks down at $N = 144$, 146 with $(2.7, 2.68) \times 10^{-4}$ in succession. The IBMC calculation for B_γ was closer to that investigation in the study of [58].

Table 3. The calculated $B(E2)$ values in e^2b^2 unit, the available experimental data [48] of $B(E2;2_1^+ \to 0_1^+)$ equal to 2.4955(437), 2.5420(974) for ^{238,240}Pu isotopes and $B(E2;2_2^+ \to 0_1^+)$, $B(E2;2_2^+ \to 4_1^+)$ equal to 0.0341(105), 0.0271(875), respectively, for ^{238}Pu isotope

Transition	^{236}Pu			^{238}Pu			^{240}Pu		
$J_i^+ \to J_f^+$	IBM	IBMC	IBMCQ	IBM	IBMC	IBMCQ	IBM	IBMC	IBMCQ
$2_1^+ \to 0_1^+$	2.3975	2.3975	2.3975	2.4827	0.4827	2.4827	2.5374	2.5374	2.5374
$4_1^+ \to 2_1^+$	3.3856	3.3856	3.3856	3.5108	3.5108	3.5108	3.5925	3.5925	3.5925
$6_1^+ \to 4_1^+$	3.6507	3.6507	3.6507	3.7958	3.7958	3.7958	3.8926	3.8926	3.8926
$8_1^+ \to 6_1^+$	3.7032	3.7032	3.7032	3.8660	3.8660	3.8660	3.9778	3.9778	3.9778
$10_1^+ \to 8_1^+$	3.6448	3.6448	3.6448	3.8266	3.8266	3.8266	3.9553	3.9553	3.9553
$12_1^+ \to 10_1^+$	3.5097	3.5097	3.5097	3.7132	3.7132	3.7132	3.8617	3.8617	3.8617
$14_1^+ \to 12_1^+$	3.3129	3.3129	3.3129	3.5411	3.5411	3.5411	3.7125	3.7125	3.7125
$16_1^+ \to 14_1^+$	3.0619	3.0619	3.0619	3.3181	3.3181	3.3181	3.5159	3.5159	3.5159
$18_1^+ \to 16_1^+$	2.7608	2.7608	2.7608	3.0487	3.0487	3.0487	3.2762	3.2762	3.2762
$20_1^+ \to 18_1^+$	2.4124	2.4124	2.4124	2.7355	0.7355	2.7355	2.9962	2.9962	2.9962
$22_1^+ \to 20_1^+$	2.0180	2.0180	2.0180	2.3800	2.3800	2.3800	2.6776	2.6776	2.6776
$24_1^+ \to 22_1^+$	1.5790	1.5790	1.5790	1.9835	1.9835	1.9835	2.3214	2.3214	2.3214
$26_1^+ \to 24_1^+$	1.0960	1.0960	1.0960	1.5468	1.5468	1.5468	1.9286	1.9286	1.9286
$28_1^+ \to 26_1^+$	0.5695	0.5695	0.5695	1.0704	1.0704	1.0704	1.4997	1.4997	1.4997
$30_1^+ \to 28_1^+$	–	–	–	0.5547	0.5547	0.5547	1.0351	1.0351	1.0351
$2_2^+ \to 0_1^+$	0.0010	0.0020	0.0002	0.0011	0.0002	0.0002	0.0012	0.0002	0.0002
$2_2^+ \to 2_1^+$	0.0015	0.0002	0.0002	0.0017	0.0003	0.0003	0.0019	0.0003	0.0003
$2_2^+ \to 4_1^+$	0.0001	0.0005	0.0005	0.0001	0.0006	0.0006	0.0001	0.0006	0.0006
$2_2^+ \to 0_2^+$	0.0175	1.9464	1.9468	0.0162	2.0447	2.0451	0.0147	2.1164	2.1166
$4_2^+ \to 2_2^+$	1.1262	2.7424	2.7438	1.1857	2.8863	2.8874	1.2292	2.9919	2.9929
$2_3^+ \to 4_1^+$	0.0005	0.0001	0.0001	0.0006	0.0001	0.0001	0.0006	0.0001	0.0001
$2_3^+ \to 2_1^+$	0.0002	0.0015	0.0015	0.0003	0.0017	0.0017	0.0003	0.0018	0.0019
$3_1^+ \to 4_1^+$	0.0009	0.0009	0.0009	0.0010	0.0009	0.0009	0.0010	0.0010	0.0010
$3_1^+ \to 2_1^+$	0.0017	0.0017	0.0017	0.0019	0.0019	0.0019	0.0021	0.0021	0.0021
$3_1^+ \to 2_2^+$	3.4285	0.0278	0.0272	3.6016	0.0250	0.0245	3.7278	0.0220	0.0217

3.3. Potential Energy Surface

Starting from the classical limit of Hamiltonian, the Potential Energy Surfaces (PESs) as a function of two deformation parameters β and γ have been written [31]:

$$E(\beta\gamma) = \frac{N_B}{1+\beta^2}\left(g_1 + g_2\beta^2\right) + \frac{N_B(N_B-1)}{(1+\beta^2)^2} \times \left(g_3\beta^4 + g_4\beta^3\cos 3\gamma + g_5\beta^2 + g_6\right), \quad (13)$$

where N_B represents the total number of bosons and $g_i (i = 1 \text{ to } 6)$ are the linear combinations of the model Hamiltonian parameters. With the triaxiality, the relation turns into:

$$E(\beta\gamma) = \frac{N_B}{1+\beta^2}\left(g_1 + g_2\beta^2\right) + \frac{N_B(N_B-1)}{(1+\beta^2)^2} \times \left(g_3\beta^4 + g_4\beta^3\cos 3\gamma + g_5\beta^2 + g_6\right) + \frac{N_B(N_B-1)(N_B-2)}{(1+\beta^2)^3}\left(g_7\beta^6 + g_8\beta^6\cos^2 3\gamma\right). \quad (14)$$

The deformation parameter γ is marking the orientation of nuclear shape while β is related to Bohr

Table 4. The calculated $B(E2)$ values in e^2b^2 unit, the available experimental data [48] of $B(E2;2_1^+ \to 0_1^+)$ equal to 2.6874(134), 2.7159(271) for ^{242,244}Pu isotopes respectively

Transition	^{242}Pu			^{244}Pu			^{246}Pu		
$J_i^+ \to J_f^+$	IBM	IBMC	IBMCQ	IBM	IBMC	IBMCQ	IBM	IBMC	IBMCQ
$2_1^+ \to 0_1^+$	2.3975	2.3975	2.3975	2.4827	0.4827	2.4827	2.5374	2.5374	2.5374
$2_1^+ \to 0_1^+$	2.6589	2.6589	2.6589	2.7083	0.7083	2.7083	2.7308	2.7308	2.7308
$4_1^+ \to 2_1^+$	3.7682	3.7682	3.7682	3.8415	3.8415	3.8415	3.8761	3.8761	3.8761
$6_1^+ \to 4_1^+$	4.0905	4.0905	4.0905	4.1764	4.1764	4.1764	4.2195	4.2195	4.2195
$8_1^+ \to 6_1^+$	4.1914	4.1914	4.1914	4.2892	4.2892	4.2892	4.3419	4.3419	4.3406
$10_1^+ \to 8_1^+$	4.1835	4.1835	4.1835	4.2946	4.2946	4.2946	4.3589	4.3589	4.3590
$12_1^+ \to 10_1^+$	4.1049	4.1049	4.1049	4.2313	4.2313	4.2313	4.3094	4.3094	4.3055
$14_1^+ \to 12_1^+$	3.9720	3.9720	3.9720	4.1161	4.1161	4.1161	4.2106	4.2106	4.2106
$16_1^+ \to 14_1^+$	3.7933	3.7933	3.7933	3.9576	3.9576	3.9576	4.0709	4.0709	4.0709
$18_1^+ \to 16_1^+$	3.5734	3.5734	3.5734	3.7604	3.7604	3.7604	3.8952	3.8952	3.8953
$20_1^+ \to 18_1^+$	3.3151	3.3151	3.3151	3.5276	3.5276	3.5276	3.6864	3.6864	3.6864
$22_1^+ \to 20_1^+$	3.0203	3.0203	3.0203	3.2608	3.2608	3.2608	3.4463	3.4463	3.4463
$24_1^+ \to 22_1^+$	2.6901	2.6901	2.6900	2.9614	2.9614	2.9614	3.1761	3.1761	3.1761
$26_1^+ \to 24_1^+$	2.3253	2.3253	2.3253	2.6302	2.6302	2.6302	2.8767	2.8767	2.8767
$28_1^+ \to 26_1^+$	1.9266	1.9266	1.9266	2.2677	2.2677	2.2677	2.5488	2.5488	2.5488
$30_1^+ \to 28_1^+$	1.4945	1.4945	1.4945	1.8745	1.8745	1.8745	2.1927	2.1927	2.1927
$2_2^+ \to 0_1^+$	0.0009	0.0001	0.0001	0.0008	0.0001	0.0001	0.0007	0.0001	0.0001
$2_2^+ \to 2_1^+$	0.0014	0.0002	0.0002	0.0013	0.0002	0.0002	0.0011	0.0002	0.0002
$2_2^+ \to 4_1^+$	0.0001	0.0005	0.0005	0.0001	0.0004	0.0004	0.0001	0.0004	0.0004
$2_2^+ \to 0_2^+$	0.0134	2.2399	2.2402	0.0130	2.3031	2.3033	0.0125	2.3417	2.3419
$4_2^+ \to 2_2^+$	1.3056	3.1705	3.1713	1.3460	3.2632	3.2639	1.3716	3.3208	3.3214
$2_3^+ \to 4_1^+$	0.0005	0.0001	0.0001	0.0004	0.0001	0.0001	0.0004	0.0001	0.0001
$2_3^+ \to 2_1^+$	0.0002	0.0014	0.0014	0.0002	0.0012	0.0012	0.0002	0.0011	0.0011
$3_1^+ \to 4_1^+$	0.0008	0.0008	0.0008	0.0007	0.0007	0.0007	0.0006	0.0006	0.0006
$3_1^+ \to 2_1^+$	0.0016	0.0016	0.0016	0.0014	0.0014	0.0014	0.0013	0.0012	0.0013
$3_1^+ \to 2_2^+$	3.9552	0.0203	0.0202	4.0696	0.0183	0.0182	4.1406	0.0166	0.0166

Collective Model (BCM) as [59]:

$$\beta^{\mathrm{IBM}} = \frac{A}{2.36N}\beta^{\mathrm{BCM}}, \tag{15}$$

where A, N are the mass number and neutrons number. A rotational symmetry has a sharp minimum at $\gamma = 0$ and $\beta = \sqrt{2}$, this can be achieved by minimizing Eq. (13) [27].

The rotational Hamiltonian can produce a classical limit of $SU(3)$ dynamical symmetry [26, 29, 30]:

$$E_{SU(3)}(\beta,\gamma) = a_2\left[\frac{N}{1+\beta^2}\left[5+\frac{11}{4}\beta^4\right] + \frac{N(N-1)}{(1+\beta^2)^2}\left[\frac{\beta^4}{2} + 2\sqrt{2}\beta^3\cos 3\gamma + 4\beta^2\right]\right] + a_1\frac{6N\beta^2}{1+\beta^2}. \tag{16}$$

By adding the cubic term to the Hamiltonian of $SU(3)$ dynamical symmetry, the nucleus can have

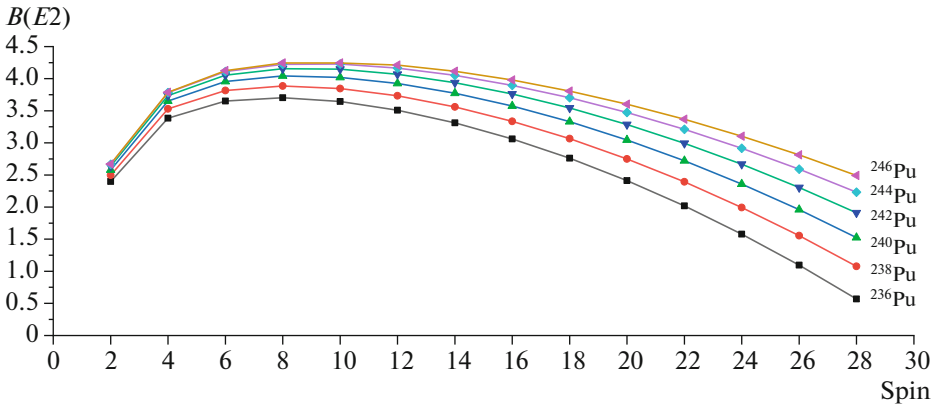

Fig. 2. Essential values of $B(E2)$ as a function of grand-band level for $^{236-246}$Pu.

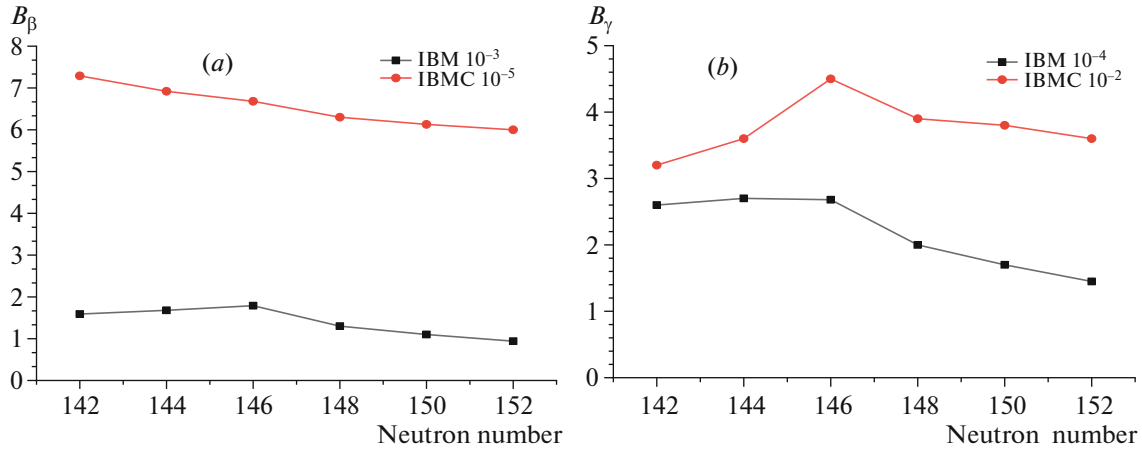

Fig. 3. Branching ratio calculation B_β (a) and $B_\gamma(b)$ as function of neutron number for $^{236-346}$Pu.

transformed in its equilibrium shapes from axial to triaxial [30]:

$$E_{SU(3)C}(\beta\gamma) = E_{SU(3)}(\beta\gamma) \qquad (17)$$
$$+\frac{\theta_3}{7}N(N-1)(N-2)\frac{\beta^6}{(1+\beta^2)^3}(-1+\cos^2 3\gamma).$$

It has been shown from the potential energy given in Eq. (16), that there are no explicitly appearing triaxial effects without included cubic d-boson term [30]. To get these effects, only the $(L = 3)$ term was chosen. We should point out, that potential energy with $SU(3)$ limit is γ-dependent this resides only in $\cos 3\gamma$ term. From Figs. 4, 5 we can see the dependence of PESs on the β and γ deformation parameters in which β ranges from 0 to 3 and γ is customary to take 0° to 60°. Additionally, the basic topology of the energy surface can be determined with and without cubic term. Note that a sign of the $\cos 3\gamma$ term in Eq. (16) is related to the value of χ in Eq. (7), thus if $\chi < 0$ it becomes a negative term, the consequence is a prolate minimum. Whereas an oblate minimum occurs when $\chi > 0$ [29]. Incidentally, Figs. 4, 5 show an example of prolate-shape nuclei, this always be desirable for several reasons; the deep minima in PESs as obtained with the IBM computations for ^{236}Pu up to ^{236}Pu are equal to ($E_{\min} = -5.213, -4.992, -4.101, -3.749, -3.720, -4.089$) in succession and all these values of PESs correspond to just $\beta = 1.5$ and $\gamma = 0°$. Moreover, it has the maxima in PESs $E_{\max} = (-0.333, -0.257, -0.106, 0.055, 0.085, 0.175)$ but these values correspond to just $\beta = 3$ and $\gamma = 45°$. This is illustrated in the first rows of Figs. 4, 5.

It is perhaps a matter that requires some consideration and attention, in which the minimum and maximum PESs values with their $\beta - \gamma$ space indicate that all the considered Plutonium isotopes have *axially symmetric shapes*. To obtain a complete picture of the potential energy surfaces for Pu isotopes, a cubic term of three-boson interactions has been added. The plots on the second rows of Figs. 4, 5 illustrate the alters of the potential energy surfaces when including the cubic interactions, we must note that the deep minima of PESs for $^{236-246}$Pu isotopes described above was without cubic term. It will be

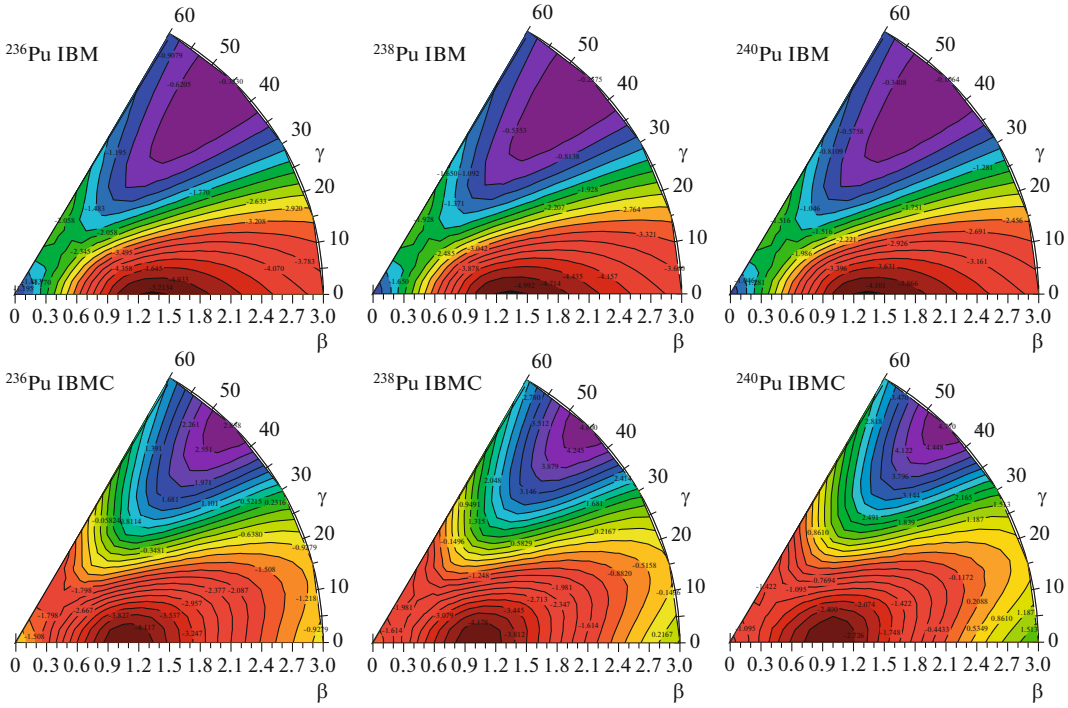

Fig. 4. Potential Energy Surfaces of $^{236-240}$Pu in $(\beta\gamma)$ plane are represented by colored contour lines. The macroscopic effects include the incidence of tension on the surfaces of potential led to prolate shape.

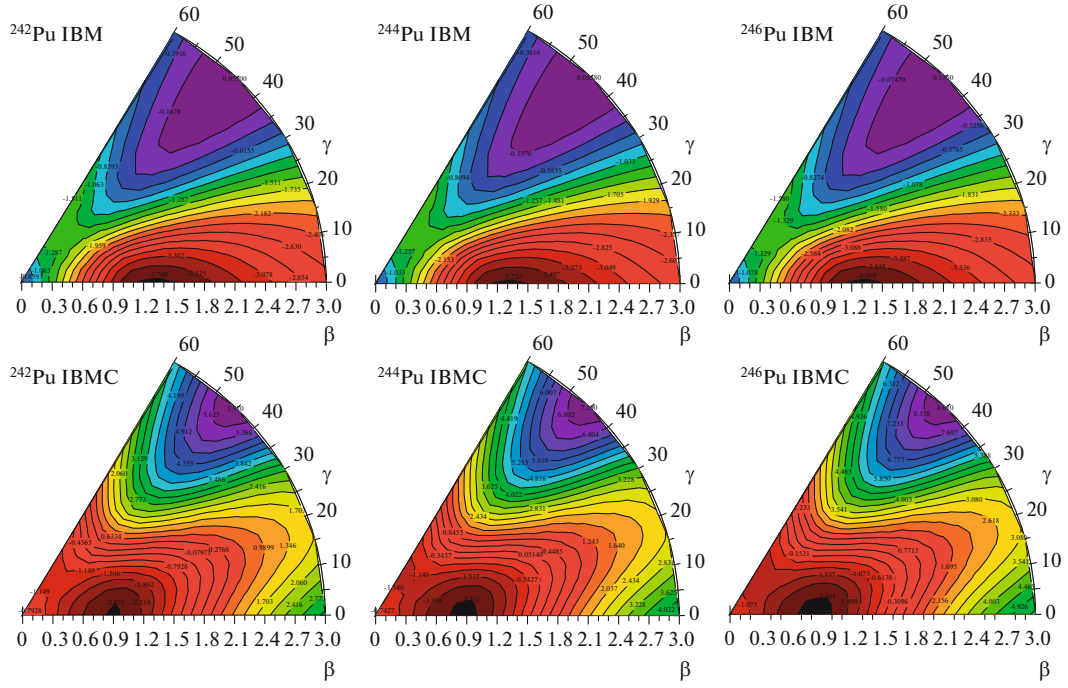

Fig. 5. As in Fig. 4 but for $^{242-246}$Pu.

after having this term, $E_{\min} = (-4.42, -4.55, -3.06, -2.58, -2.35, -2.5)$, respectively, in conformity with $\beta = 1$ and also $0° < \gamma < 15°$.

These contours have the minimum potential energy followed by other contours' line with their energies which gradually increasing. A rising in the maximum potential energies surface has been observed as a result of cubic interactions, these energies ($E_{\max} = 2.838, 4.6, 4.77, 5.97, 7.19, 8.16$) are also increasing as a function of the mass number, these maximum

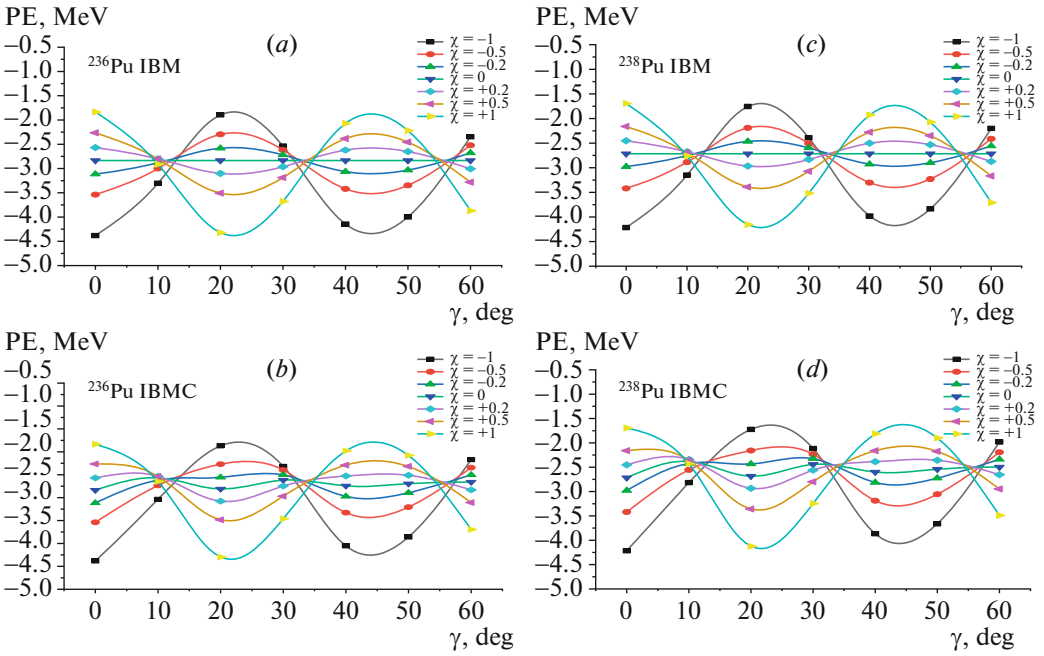

Fig. 6. (Color online) Inspection of the prolet–oblete transition for the potential energy of ^{236,238}Pu isotopes: (a, c) with $\theta_3 = 0$, (b, d) with $\theta_3 = -0.004$.

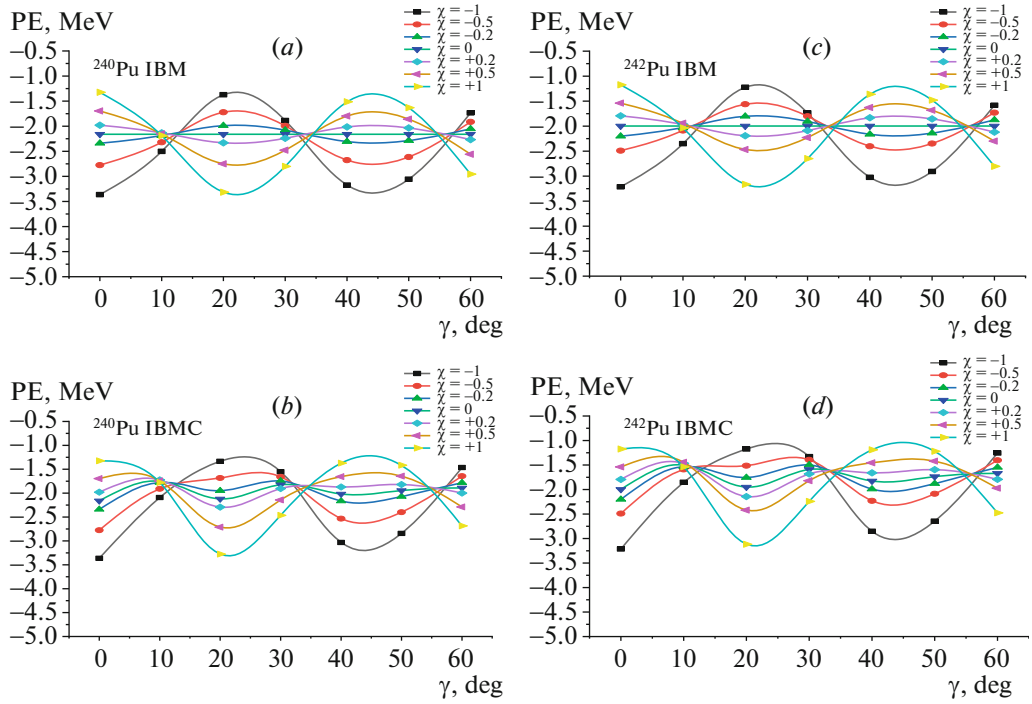

Fig. 7. As in Fig. 6, but for ^{240,242}Pu.

values seem to correspond to similar β and γ space of the maximum without cubic interactions (*axial case*) mentioned earlier. If we think more about the bold contour which is labeled by the minimum value and the other contours behind it in the second rows of Figs. 4, 5 we find it narrower compared to those contours in the first. It can be observed from the second row of Fig. 5 that there is a widening in the sharpness of a black contour line labeled by the value (−2.575) with increasing the mass number. However, it is been necessary to say that the breakdown of contour lines is due to the highly dependent term proportional to

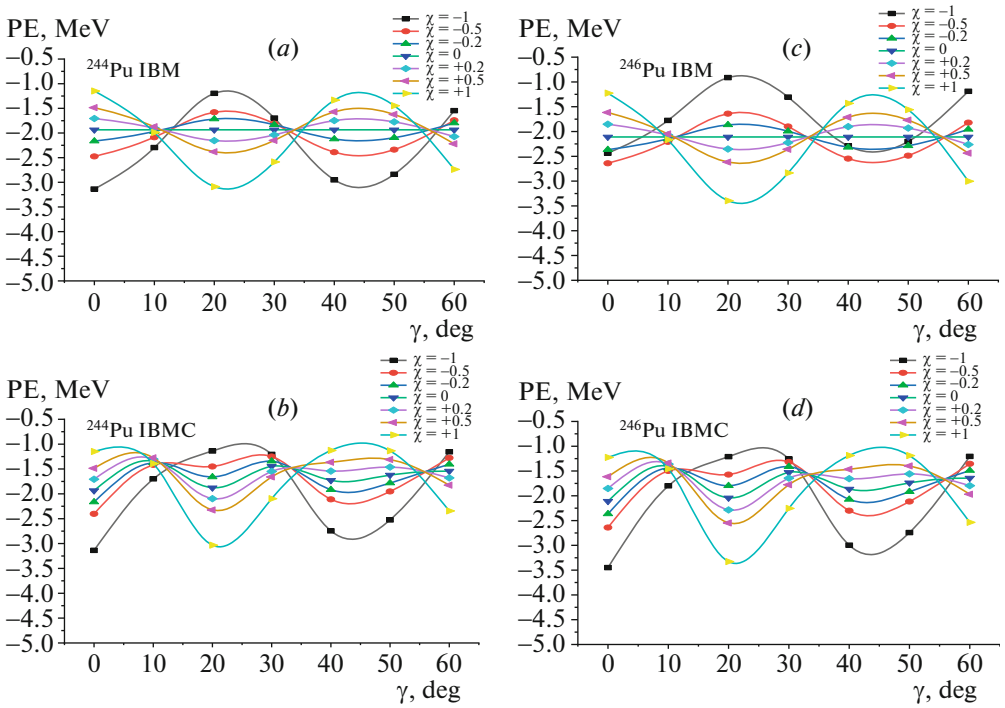

Fig. 8. As in Fig. 6, but for ^{244,246}Pu.

$\cos^2 3\gamma$. An important implication of this tendency is that it enhances the role of three-boson interactions in inducing the appearance of stable triaxial shapes on the PESs of the Plutonium chain. We think that an increase in the potential energy surface will make the Plutonium isotopes more stable and therefore improve the importance of having triaxial interactions together with that axial intrinsic in the nuclei.

In order to show the effect of the cubic term on potential energy values with different values of χ the PES values have been calculated with $0 \leqslant \gamma^0 \leqslant 60$ and $-1 \leqslant \chi \leqslant +1$. The results are summarized in Figs. 6–8. The figures show that there have been gradual changes in the shape of the nucleus and its potential form. In this investigation the one parameter of significance is a_2 in the Q operator (Eqs. (7) and (10) [59–61]. The values of χ were selected to represent $SU(3)$ *prolate* with $(\chi = -1)$ passing through an $O(6)$ $(\chi = 0)$ to $SU(3)$ *oblate* with $(\chi = +1)$. In the first rows of Figs. 6–8 we see that the potential with $\theta_3 = 0$ is γ-dependent at $(\chi = -1, -0.5, -0.2, +0.2, +0.5, +1)$ but is not at $(\chi = 0)$. In contrast, we can see in the second rows that the values of PES at $(\chi = 0)$ are γ-dependent, this is due to the three-body interactions $(\theta_3 = -0.004)$.

4. CONCLUSIONS

To summarize, we have calculated the spectra and $E2$ transition probabilities of Pu nuclei in the frame of IBM-1 plus cubic and quadruple terms. The obtained results have shown that it is instructive to introduce these terms into IBM, thus such interaction terms giving a new expansion and features to the model in some aspects. The $^{236-246}$Pu isotopes are axially symmetric at low angular momentum but at high angular momentum, they have been found in triaxial shapes. Finally, to describe the structure of the triaxial nuclei, we should consider much of the cubic terms.

REFERENCES

1. G. N. Flerov and G. M. Ter-Akopian, Rep. Prog. Phys. **46**, 817 (1983).
2. J. V. Kratz, Radiochim. Acta **32**, 25 (1983).
3. Z. Ren, Phys. Rev. C **65**, 051304(R) (2002).
4. S. C'wiok, P. H. Heenen and W. Nazarewicz, Nature (London, U.K.) **433**, 705 (2005).
5. J. H. Hamilton, S. Hofmann, and Y. T. Oganessian, Ann. Rev. Nucl. Part. Sci. **63**, 383 (2013).
6. Q.-Z. Chai, W.-J. Zhao, M.-L. Liu, and H.-L. Wang, Chin. Phys. C **42**, 054101 (2018).
7. A. Soylu, Chin. Phys. C **43**, 074102 (2019).
8. M. Schädel, J. V. Kratz, H. Ahrens, W. Brüchle, G. Franz, H. Gäggeler, I. Warnecke, G. Wirth, G. Herrmann, N. Trautmann, and M. Weis, Phys. Rev. Lett. **41**, 469 (1978).
9. H. Gäggeler, N. Trautmann, W. Brüchle, G. Herrmann, J. V. Kratz, P. Peuser, M. Schädel, G. Tittel, G. Wirth, H. Ahrens, H. Folger, G. Franz, K. Sümmerer, and M. Zendel, Phys. Rev. Lett. **45**, 1824 (1980).

10. Z. Patyk, J. Skalski, and A. Sobiczewski, Nucl. Phys. A **502**, 591 (1989).
11. D. N. Poenaru, R. A. Gherghescu, and W. Greiner, Phys. Rev. Lett. **107**, 062503 (2011).
12. S. Hofmann, Z. Phys A **358**, 125 (1997).
13. R. Smolańczuk, Phys. Rev. C **60**, 021301(R) (1999).
14. Z. Zhong-Zhou, Chin. Phys. C **30**, 47 (2006).
15. D. S. Delion, A. Sandulescu, and W. Greiner, Phys. Rev. C **69**, 044318 (2004).
16. C. Karthikraj and Z. Ren, Phys. Rev. C **101**, 014603 (2020).
17. Z.-H. Zhang, J. Meng, E.-G Zhao, and S.-G Zhou, Phys. Rev. C **87**, 054308 (2013).
18. M. S. Nadirbekov, S. N. Kudiratov, and F. N. Temirov, Phys. At. Nucl. **83**, 841 (2020).
19. A. Arima and F. Lachello, Ann. Phys. (N.Y.) **99**, 253 (1976).
20. A. Arima and F. Lachello, Ann. Phys. (N.Y.) **111**, 201 (1978).
21. A. Arima and F. Lachello, Ann. Phys. (N.Y.) **123**, 468 (1979).
22. F. Iachello and A. Arima, *The Interacting Boson Model* (Cambridge Univ. Press, UK, 1987).
23. L. Wilets and M. Jean, Phys. Rev. **102**, 788 (1956).
24. N. Bohr and B. Mottelson, Mat. Fys. Medd. Dan. Vid. Selsk. **16**, 27 (1953).
25. J. N. Ginocchio and M. W. Kirson, Phys. Rev. Lett. **44**, 1744 (1980).
26. A. E. L. Dieperink and O. Scholten, Nucl. Phys. A **346**, 125 (1980).
27. A. E. L. Dieperink, O. Scholten, and F. Iachello, Phys. Rev. Lett. **44**, 1747 (1980).
28. A. E. L. Dieperink, Prog. Part. Nucl. Phys. **9**, 121 (1983).
29. J. N. Ginocchio and M. W. Kirson, Nucl. Phys. A **350**, 31 (1980).
30. P. Van Isacker and J.-Q. Chen, Phys. Rev. C **24**, 684 (1981).
31. K. Heyde, P. van Isacker, M. Waroquier, and J. Moreau, Phys. Rev. C **29**, 1420 (1984).
32. A. E. L. Dieperink and R. Bijker, Phys. Lett. B **116**, 77 (1982).
33. B. Sorgunlu and P. Van Isacker, Nucl. Phys. A **808**, 27 (2008).
34. V. Miguel, R. Flores-Mendieta, and J. Herńandez, (2021, unpublished).
35. G. Maino, Heavy Ion Phys. **16**, 419 (2002).
36. E. Canetta and G. Maino, Phys. Lett. B **483**, 55 (2000).
37. N. Al-Dahan, Chin. Phys. C **41**, 064105 (2017).
38. N. Bohr and B. Mottelson, Mat. Fys. Medd. Dan. Vid. Selsk. **14**, 26 (1952).
39. B. R. Barrett, Lect. Notes Phys. **180**, 407 (1983).
40. F. Iachello, *Dynamic Symmetries in Nuclei* (Int. Atomic Energy Agency, Japan, 1982), Vol. 15.
41. R. F. Casten and D. D. Warner, Rev. Mod. Phys. **60**, 389 (1988).
42. A. Leviatan, J. E. García-Ramos, and P. Van Isacker, Phys. Rev. C **87**, 021302(R) (2013).
43. V. Werner, N. Pietralla, P. von Brentano, R. F. Casten, and R. V. Jolos, Phys. Rev. C **61**, 021301(R) (2000).
44. P. van Isacker, Phys. Rev. Lett. **83**, 4269 (1999).
45. D. J. Rowe and G. Thiamova, Nucl. Phys. A **760**, 59 (2005).
46. G. Thiamova and P. Cejnar, Nucl. Phys. A **765**, 97 (2006).
47. G. Thiamova, Eur. Phys. J. A **45**, 81 (2010).
48. ENSDF. http://www.nndc.bnl.gov/ensdf. Accessed 2020.
49. D. D. Warner and R. F. Casten, Phys. Rev. C **25**, 2019 (1982).
50. D. D. Warner and R. F. Casten, Rev. Lett. **48**, 1385 (1982).
51. P. Van Isacker, The Software Package IBM-1 and IBMT Computer Codes.
52. E. A. McCutchan, D. Bonatsos, N. V. Zamfir, and R. F. Casten, Phys. Rev. C **76**, 024306 (2007).
53. R. F. Casten, P. von Brentano, and A. M. I. Haque, Phys. Rev. C **31**, 1991(R) (1985).
54. J. P. Elliott, Rep. Prog. Phys. **48**, 171 (1985).
55. O. Scholten, F. Iachello, and A. Arima, Ann. Phys. (N.Y.) **115**, 225 (1978).
56. H. H. Kassim, A. A. Mohammed-Ali, F. I. Sharrad, I. Hossain, and K. S. Jassim, Iran J. Sci. Technol. Trans. Sci. **42**, 993 (2018).
57. J. P. Draayer and C. S. Han, Lect Notes Phys **135**, 349 (1980).
58. G. Puddu and O. Scholten, Nucl. Phys. A **348**, 109 (1980).
59. P. Cejnar, J. Jolie, and R. F. Casten, Rev. Mod. Phys. **82**, 2155 (2010).
60. R. L. Gill, W. T. Chou, and R. F. Casten, Nucl. Phys. A **542**, 32 (1992).
61. J. Jolie, R. F. Casten, P. von Brentano, and V. Werner, Phys. Rev. Lett. **87**, 162501 (2001).